How to Use Lasers for Imaging Attosecond Dynamics of Nuclear Processes

Nenad Milosevic,[1] Paul B. Corkum,[2] and Thomas Brabec[1,*]

[1]*Center for Photonics Research, University of Ottawa, Ottawa, Ontario, Canada K1N 6N5*

[2]*Steacie Institute of Molecular Sciences, National Research Council, Ottawa, Ontario, Canada K1A 0R6*

(Received 30 May 2003; published 8 January 2004)

We identify a laser configuration in which attosecond electron wave packets are ionized, accelerated to multi-MeV energies, and refocused onto their parent ion. Magnetic focusing of the electron wave packet results in return currents comparable with large scale accelerator facilities. This technique opens an avenue towards imaging attosecond dynamics of nuclear processes.

DOI: 10.1103/PhysRevLett.92.013002 PACS numbers: 32.80.–t, 24.90.+d, 34.80.Dp

High laser intensity atomic and molecular physics is dominated by the recollision between an ionized electron and its parent ion. The electron is ionized near the peak of the laser field, accelerated away from the ion, and driven back to its parent ion once the field direction reverses. Recollision leads to nonsequential double ionization, high harmonic generation, and attosecond extreme ultraviolet and electron pulses [1].

In contrast, at relativistic intensities and with a single propagating laser beam, the Lorentz force pushes the electron in the direction of the wave vector. The forward motion exceeds the size of the returning wave packet for intensities greater than 10^{16} W/cm^2 (at 800 nm) preventing recollision. Thus, efficient recollision is confined to electron energies <1 keV [2,3]. The extension of laser induced recollision physics to relativistic energies is a long-standing and to-date unsolved issue.

The first major result of this Letter is a solution to this problem. We show that the Lorentz force is eliminated for two counterpropagating, equally handed, circularly polarized beams throughout the whole focal volume, as long as the laser pulses are sufficiently long. In this configuration, the recollision energy is limited only by the maximum achievable laser intensity (currently $\approx 10^{23}$ W/cm^2).

The second major result is magnetic focusing of the electron wave packet. As the laser magnetic field opposes the electron wave packet spread, return currents in excess of 10^{11} A/cm^2 can be realized, comparable with the currents achieved in large scale electron accelerator facilities. We show that the currents are sufficient to excite nuclear reactions and deeply bound core electrons. Ultrahigh intensity laser pulses interacting with plasmas can also produce relativistic particles that induce nuclear processes [4]. However, the ultrafast collision times cannot be used for time resolved spectroscopy, as the interaction between the particles cannot be timed.

The third major result is the potential for attosecond laser electronuclear (and core hole) spectroscopy (ALENS), enabled by the asec duration of the returning electron wave packet. We show that the asec "streak-camera" methods demonstrated recently experimentally [5,6] are also applicable in the relativistic regime. ALENS will yield novel insight into fundamental nuclear properties, as discussed near the end of this Letter.

Recently, a number of methods for the suppression of the Lorenz force were proposed [3]. All suffer from the limit that the Lorenz force is eliminated only over a small fraction of the standing wave. The portion where recollision can occur decreases with increasing laser intensity. Our technique eliminates the Lorenz force over the whole focal region. This is achieved by two equal-handed, counterpropagating, circularly polarized laser pulses (see Fig. 1). In the following, we will show that this field configuration makes ALENS possible.

The electron current of the returning electron is calculated by a relativistic generalization of the semiclassical two-step model [7]. The calculations are performed for hydrogenlike ions with various charge states Z. The ionization potential [8] is given by $I_p = mc^2[1 - \sqrt{1 - (\alpha Z)^2}]$, where α, m, and c denote the fine structure constant, the electron mass, and the vacuum light velocity, respectively. In the first step, the electron is born in the continuum. From this point electron trajectories are launched, with the center trajectory having zero birth velocity along the laser electric field axis. The trajectories

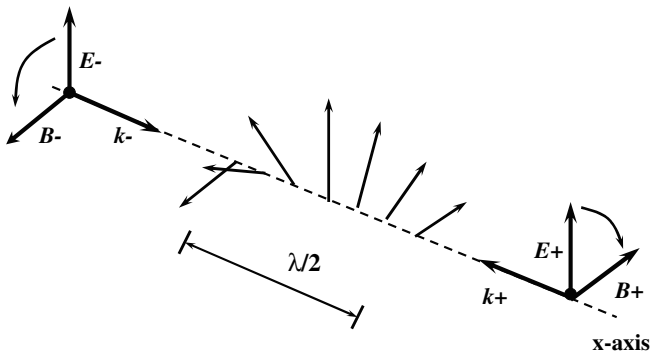

FIG. 1. Schematic of the laser setup consisting of two equal handed, circularly polarized, counterpropagating laser pulses with equal intensities. Electric and magnetic fields are parallel, point along the arrows, rotate in space along the propagation axis, and vary sinusoidal in time and 90° out of phase.

are weighted with the quantum mechanical velocity distribution of the ionized electron wave packet. Ionization probability and velocity distribution are taken from an analytical solution of the Dirac equation [8]. The trajectories are propagated by solving the classical relativistic equations of motion—spin effects and the motion of the parent ion are neglected. Both effects are small in the parameter regime considered here [9]. The electron current is determined by the number of trajectories revisiting the parent nucleus.

Figure 2(a) shows the returning electron current, as seen by the parent ion, versus time for the configuration in Fig. 1 and for a laser peak intensity of 10^{21} W/cm^2. The electron pulse width is 250 asec and the peak current density is 10^{10} A/cm^2. The surprisingly strong electron current comes from the fact that in our configuration the magnetic field is directed (anti)parallel to the electric field. This field configuration focuses parts of the electron wave packet, thus opposing quantum diffusion. As a result, the electron energy distribution is different from the nonrelativistic case, as is shown in Figs. 2(a) and 2(b). In the nonrelativistic limit, electrons with low energies have the highest return probability [5]. Here low energy components are suppressed and high energy components are enhanced due to magnetic focusing.

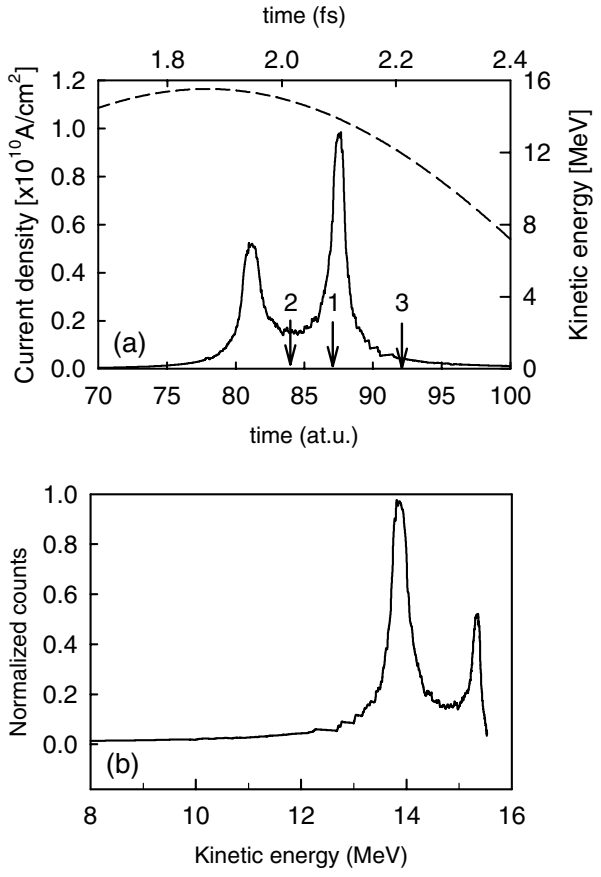

FIG. 2. (a) Current of the returning electron versus time (full line). The arrows are associated with Fig. 3; kinetic energy of the returning electron versus time (dashed line). (b) Spectrum of the returning electron pulse. The parameters are laser peak intensity $I = 10^{21}$ W/cm^2, wavelength $\lambda = 800$ nm. The laser electric field is described by a (plane wave) cos-carrier, i.e., is maximum at time $t = 0$; hydrogenlike ion, $Z = 15$, $I_p = 3.1$ keV.

The magnetic field focuses the electron by superimposing a cyclotronlike motion onto its trajectory along the electric field [10]. Optimum focusing occurs, when the time for a round-trip in the y-z plane is equal to the electron excursion time along the x axis. This is demonstrated in Fig. 3, where the $1/e$ width of the returning electron wave function is plotted for the return times marked with an arrow in Fig. 2. The maximum current in Fig. 2 corresponds to the wave packet in Fig. 3 that experiences strongest focusing. The asymmetry and the rotation of the returning wave packet come mainly from the change of direction of the laser electric field along the x direction.

As pointed out in the beginning, relativistic recollision is insensitive to subwavelength variations of the laser electric and magnetic carrier wave, and therefore works perfectly along the whole x axis in the limit of plane waves. However, finite laser pulse durations limit the interval along the z axis at which recollision can take place. Recollision remains unaffected at the point at which the propagation distance of the counterpropagating pulses is equal ($x = 0$). Away from this point, a growing intensity difference between the two counterpropagating waves arises. The resulting elliptic polarization offsets the returning electron wave packet and reduces the current. Our calculations show that the tolerance level for recollision to occur lies at a peak intensity difference of $\approx 0.5\%$ between the counterpropagating waves, independent of the absolute value of the peak intensity. Hence,

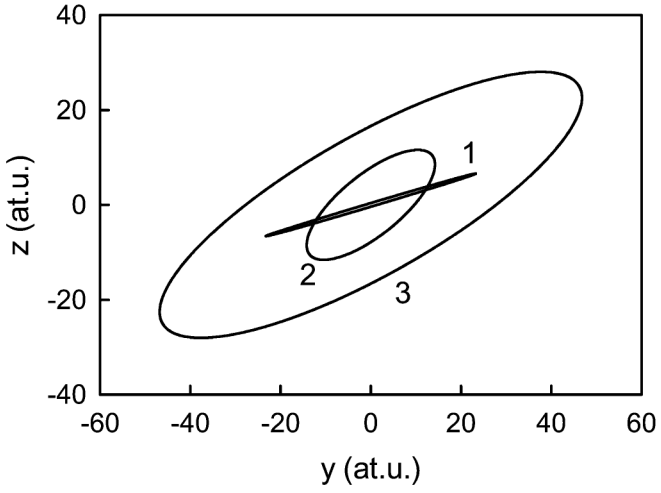

FIG. 3. Same parameters as in Fig. 2; the numbers refer to the numbers in Fig. 2. The full lines denote the $1/e$ width of the transversal electron wave packet at t_r. The three wave packets have birth times, $t_{b1} = 7.3$ a.u., $t_{b2} = 8.2$ a.u., and $t_{b3} = 5.9$ a.u., and return times $t_{r1} = 87$ a.u., $t_{r2} = 84$ a.u., and $t_{r3} = 92$ a.u.

the laser pulse shape determines the interaction length. The interaction volume depends sensitively on the flatness of the laser envelope and is optimized for a flat top profile. Experimentally, optimization can be realized by broad bandwidth pulses in combination with adaptive techniques [11].

We repeated the calculations of Fig. 2 for ions with charge states ranging from $Z = 1$ to 30. The results are depicted in Figs. 4(a) and 4(b). For charge states below $Z = 10$, the influence of magnetic focusing drops rapidly and disappears completely at $Z = 5$, which is around the onset of relativistic effects. The increase of the return current for $Z < 5$ is due to the decrease of the transversal spread of the electron wave packet on the one hand, and due to Coulomb focusing [7] on the other hand. Apart from minor changes in the return time and in the electron pulse shape, the returning electron pulse is insensitive to the particular choice of parameters. The pulse duration between $Z = 15$ and $Z = 30$ ranges between 100 and 300 asec. Finally, from $Z = 15$ to $Z = 30$, electron return energies between 10 and 100 MeV are realized.

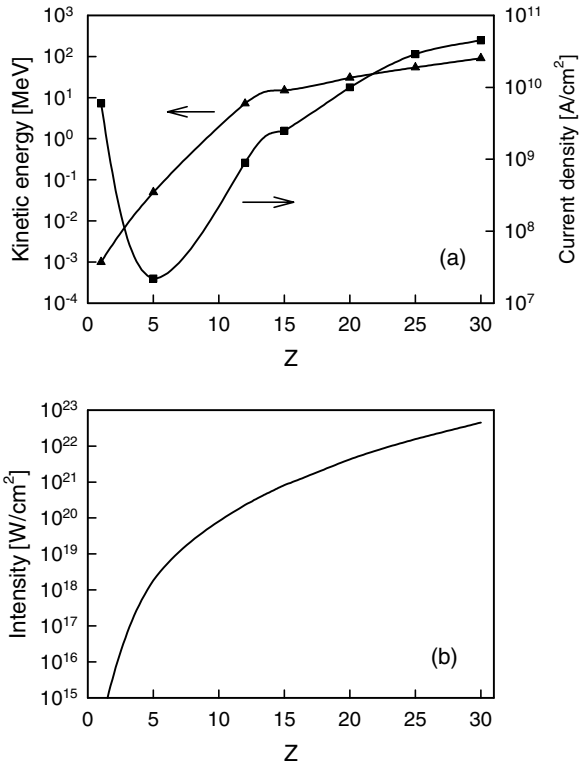

FIG. 4. (a) Volume averaged electron current density and electron kinetic energy versus ion charge state Z; (b) laser peak intensity versus Z. Peak laser intensity in (b) was chosen to ionize 80% of the ion; other parameters: super-Gaussian pulse shape with 40 fs FWHM duration, wavelength $\lambda =$ 800 nm. The return energy and the peak current have been averaged over the interval $x = \pm 1$ μm, where recollision takes place. Note that the averaged current is smaller than the non-averaged current depicted in Fig. 2(a).

To demonstrate the possibility of ALENS, we calculated the electronuclear excitation of continuum states in Xe, based on the parameters and results of Fig. 4. Our estimate is representative for a broad range of nuclei, as the continuum excitation cross section depends only weakly on the specific choice of nucleus. The excitation rate was determined from the photonuclear cross section [12] by transforming the electron current into virtual photons following the Williams-Weizsäcker method [13]. For $Z = 20$ (10^{22} W/cm^2), a laser repetition rate of 1 kHz and a pulse duration of 40 fs, 10^{-10} continuum transitions per ion, per second, are obtained. Assuming a laser pulse area of 500 μm^2, an interaction length of 2 μm, and a gas density of 10^{15} cm^{-3}, the number of ions in the interaction volume is 10^7. This gives $\approx 10^{-3}$ (coherent) continuum transitions per second coming from recollisions with parent ions. The (incoherent) continuum transitions coming from collisions of electrons with the other ions are estimated to be $\approx 5 \times 10^{-6}$ and can be neglected.

Nuclear decay changes the mass and/or charge of the nucleus. This pronounced event can be measured with a detection efficiency of close to unity in an isotopically pure gas. As a result, at a kHz repetition rate, one nuclear decay can be measured every 15 min. Note that the number of coherent continuum transitions remains unchanged as long as the product of gas density and repetition rate is kept constant. Lower repetition rates can be used by increasing the gas density. However, at higher gas densities, the noise background coming from incoherent collisions increases. Coherent and incoherent contributions become comparable at ≈ 1 Hz.

The correlation between electron and laser field opens the way to pump-probe ALENS experiments. The electron pulse returns at a fixed, known time within a laser half cycle to its parent ion and pumps the nucleus to an excited state. For charged particle emission, the time of decay t_d can be determined by using the laser field to streak the energy of the fragment. This is a direct analogy with the way attosecond optical pulses are measured [6]. For a fragment with charge Ze the momentum, $\mathbf{P} = \mathbf{Q} - Ze\mathbf{A}(t_d)$, consists of a field-free contribution, $\mathbf{Q}$, and of a component coming from the laser electric field $\mathbf{E}$ with $-d\mathbf{A}/dt = \mathbf{E}$. At a laser intensity of 10^{23} W/cm^2 and a wavelength of 800 nm, the drift energy is 1 MeV for a proton. The laser induced momentum change depends on whether the decay takes place in a half cycle with positive or negative vector potential. This causes a structure in the energy spectrum of the fragments from which the instant of decay can be retrieved. For example, along the laser vector potential a double peaked spectrum is created. The distance between the peaks is determined by $A(t_d)$ from which t_d can be obtained.

Because the process of ionization and recollision is repeated each 1/2 cycle, the largest time resolution with unchirped laser pulses is 1/2 laser period. However, if the counterpropagating pulses are oppositely chirped, the

number of recollisions can be controlled. With the appropriate chirp, only one recollision occurs across the full focal volume at the same time. In this configuration the time of measurement can be extended beyond 1/2 cycle.

Thus far, the lower limit to the time resolution is set by the duration of the electron pulse. The correlation [5] between the laser field and the electron pulse can be used to go beyond this limit. Just as the field labels the time of decay of the nucleus, it also labels the time of recollision of the electron. In this way, the laser field synchronizes the time of nuclear excitation and decay. We can determine the birth (t_b) and recollision (t_r) time of the electron from energy conservation, $W_0 = W + \sum_i W_i + I_n$. Here, W_0 and W denote the kinetic energy of the electron before and after recollision, respectively. The kinetic energy of fragments and nucleus, $\sum_i W_i$, is obtained from measurement, and I_n is the nuclear binding energy. By inserting $W_0 = c\sqrt{e^2[A(t_b) - A(t_r)]^2 + mc^2}$ and $W = c\sqrt{[\mathbf{q} - e\mathbf{A}(t_r)]^2 + mc^2}$, and by using the fact that t_b is a function of t_r, we obtain an equation determining t_r. The final electron momentum $\mathbf{q}$ must be determined from measurement also. As the electron transfers momentum to the nucleus, it gains a momentum in the plane perpendicular to the electric field by which it can be distinguished from the other electrons quivering predominantly along the electric field. When the electron recollision time is known, the lower limit of time resolution is determined by the longitudinal momentum uncertainty at electron birth. Our calculations show that this is on the order of 1 asec.

We have introduced a method that dramatically changes how the laser fields interact with charged particles. It will alter the physics anywhere relativistic laser fields interact with electrons. We have emphasized its potential for time resolving nuclear dynamics. The technique is equally important for time resolving deeply bound core hole dynamics. In nuclear physics it opens novel possibilities. For example, the study of decay and damping of nuclear dynamical processes, such as giant resonances, is an important issue in electronuclear physics. It reveals information on fundamental nuclear properties, such as dissipation and viscosity in nuclei, and presents an important test bed for theoretical many body nuclear physics [14]. Collective modes decay into compound nuclear states and into a continuum of escaping states leading to nuclear particle emission and/or fission. One expects a hierarchy of lifetimes linked to a hierarchy of energy scales starting from a few MeV associated with collective states to a few eV being characteristic of long-lived compound nuclear states.

To date, there exist few tools for the direct time measurement of fast nuclear dynamics. One exception is the crystal blocking technique used for the measurement of fission times. It has a time resolution between 10^{-19} s and 10^{-16} s [15]. The measured decay times with this method are much longer than the time scales obtained from indirect techniques [15]. Other decay processes such as neutron and proton emission have been accessed by spectral measurements only [16]. Spectral measurements cannot give accurate information on the lifetime, because of the missing phase information. Furthermore, the spectral resolution is limited to the keV range, i.e., to time scales $<10^{-18}$ s. ALENS promises to yield new insight into nuclear dynamics by (i) supplying direct time information and (ii) by giving access to the asec/fs (sub-keV/eV) range that cannot be accessed by spectral means.

Finally, high repetition rates are the key to making ALENS practical. Since during one pass only a tiny fraction of the laser energy is used, the same laser pulse can be focused multiple times into the interaction volume. Such schemes can increase the repetition rate by orders of magnitude.

This research was supported by the Austrian FFWF, Grant No. Y142-TPH.

*Electronic address: brabec@uottawa.ca

[1] T. Brabec and F. Krausz, Rev. Mod. Phys. **72**, 545 (2000); "Strong Field Laser Physics," edited by T. Brabec and H. Kapteyn (to be published).
[2] M. Walser, C. H. Keitel, A. Scrinzi, and T. Brabec, Phys. Rev. Lett. **85**, 5082 (2000); J. S. Roman, L. Roso, and H. R. Reiss, J. Phys. B **33**, 1869 (2000).
[3] J. R. Vazquez de Aldana and L. Roso, J. Opt. Soc. Am. B **19**, 1467 (2002); N. J. Kylstra *et al.*, Phys. Rev. Lett. **85**, 1835 (2000).
[4] K. W. D. Ledingham, P. McKenna, and R. P. Singhal, Science **300**, 1107 (2003); T. E. Cowan *et al.*, Phys. Rev. Lett. **84**, 903 (2000).
[5] H. Niikura, *et al.*, Nature (London) **417**, 917 (2002); H. Niikura *et al.*, Nature (London) **421**, 826 (2003).
[6] M. Drescher *et al.*, Nature (London) **419**, 803 (2002); A. Baltuska *et al.*, Nature (London) **421**, 611 (2003).
[7] T. Brabec, M. Yu. Ivanov, and P. B. Corkum, Phys. Rev. A **54**, R2551 (1996).
[8] N. Milosevic, V. P. Krainov, and T. Brabec, J. Phys. B **35**, 3515 (2002).
[9] M. W. Walser, C. Szymanowski, and C. H. Keitel, Europhys. Lett. **48**, 533 (1999).
[10] T. Zuo *et al.*, Phys. Rev. A **51**, 3991 (1995); D. B. Milosevic and A. F. Starace, Phys. Rev. Lett. **82**, 2653 (1999).
[11] N. Dudovich, D. Oron, and Y. Silberberg, Nature (London) **418**, 512 (2002).
[12] Nuclear data viewer: t2.lanl.gov/data/ndviewer.html
[13] J. D. Jackson, *Classical Electrodynamics* (Wiley, New York, 1998), 3rd ed.
[14] G. F. Bertsch, P. F. Bortignon, and R. A. Broglia, Rev. Mod. Phys. **55**, 287 (1983).
[15] F. Goldenbaum *et al.*, Phys. Rev. Lett. **82**, 5012 (1999); I. Gontchar, M. Morjean, and S. Basnary, Europhys. Lett. **57**, 355 (2002).
[16] H. Diesener *et al.*, Phys. Rev. Lett. **72**, 1994 (1994); S. Strauch *et al.*, Phys. Rev. Lett. **85**, 2913 (2000).